Journal of Alloys and Compounds 520 (2012) 207–212

Contents lists available at SciVerse ScienceDirect

Journal of Alloys and Compounds

journal homepage: www.elsevier.com/locate/jallcom

Hydrogen storage properties of Mg–Ni–Fe composites prepared by hydriding combustion synthesis and mechanical milling

Yunfeng Zhu*, Yang Yang, Lingjun Wei, Zelun Zhao, Liquan Li

College of Materials Science and Engineering, Nanjing University of Technology, Nanjing 210009, People's Republic of China

ARTICLE INFO

Article history:
Received 30 November 2011
Received in revised form
28 December 2011
Accepted 4 January 2012
Available online 11 January 2012

Keywords:
Hydrogen storage
Mg–Ni–Fe composite
Hydriding combustion synthesis
Mechanical milling

ABSTRACT

We reported the structures and superior hydrogen storage properties of the composites $Mg_{90}Ni_{10-x}Fe_x$ (x = 0, 2, 4, 6 and 8) prepared by the process of HCS + MM, i.e., the hydriding combustion synthesis followed by mechanical milling. By means of X-ray diffraction (XRD), scanning electron microscopy (SEM) with an energy dispersive X-ray spectrometer (EDX) and gas reaction controller (GRC), the crystal structures, surface morphologies and hydriding/dehydriding properties of the composites were studied in detail. The $Mg_{90}Ni_{10-x}Fe_x$ (x = 2, 4, 6 and 8) composites consist of MgH_2, Mg, Mg_2NiH_4, $Mg_2NiH_{0.3}$ and Fe phases, while $Mg_{90}Ni_{10}$ is composed of MgH_2, Mg, Mg_2NiH_4 and $Mg_2NiH_{0.3}$. It is found that $Mg_{90}Ni_2Fe_8$ has the best hydriding properties, requiring only 30 s to absorb 97% of its saturated hydrogen capacity of 4.80 wt.% at 373 K. The best dehydriding result is obtained with $Mg_{90}Ni_8Fe_2$, which desorbs 2.02 and 4.40 wt.% hydrogen at 493 and 523 K, respectively. The microstructures of the composites prepared by HCS + MM have remarkable influences on the enhanced hydriding/dehydriding properties. In addition, the catalytic effects of Mg_2Ni and Fe phases during hydriding/dehydriding were discussed in this study.

1. Introduction

Nowadays, the primary energy sources including coal, natural gas, and petroleum are being severely challenged in meeting the energy and environmental needs, there is an increasing need for new and greater sources of energy for future global transportation applications. Hydrogen has been considered as an ideal substitute to traditional fossil fuels, but the storage of hydrogen for application faces strong obstacles today [1]. Hydrogen storage by solid state materials is considered as a promising way, which can be used in nickel-metal hydride secondary batteries and fuel cell vehicles [2–11]. Mg and Mg-based materials are regarded as promising candidates for vehicular hydrogen storage owning to their high hydrogen storage capacities, low price, abundant resources and friendly to environment [12–15]. Unfortunately, Mg has a high thermodynamic stability (the enthalpy of hydride formation for Mg is −74 kJ/mol) [16] and a lower plateau pressure at room temperature. Besides, Mg usually absorbs and desorbs hydrogen at relatively high temperature and with slow kinetics. So far, extensive attempts have been made to improve the hydrogen absorption/desorption behavior of Mg.

Compositional optimization of Mg-based alloys has been proved to be an effective way to improve the hydrogen storage properties. These investigations can be classified into two directions. One is alloying of other metals with Mg such as Mg–Ni [17,18], Mg–La–Cu [19], Mg–Mn–Ni [20], Mg–Al [21], Mg–Fe [22], Mg–La [23], Mg–Co [24,25] and so on. The other is preparing Mg-based composites including Mg-metals (Mg–Nb [26], Mg–Ni–Cu [27], Mg–Ni–V [28], Mg–Ni–Fe [29–31]), Mg-oxides (Mg–Fe_2O_3 [32], Mg–Nb_2O_5 [33], Mg–Cr_2O_3 [34]), Mg-intermetallics (Mg–$LaNi_5$ [35], Mg–TiVMn [36], Mg–FeTi [37], Mg–ZrFeCr [38]), Mg-carbon [39,40], and so on. Among these systems, Mg–Ni–Fe is one of the attractive hydrogen storage materials. Bobet et al. [29] reported that Mg–Ni–Fe nanocomposite has better hydriding and dehydriding properties than that of the nanocomposite without Fe.

Some material processing techniques have also been proved to be able to improve the hydrogen storage properties of Mg-based alloys, such as melt spinning [41], mechanical milling (MM) [42–44] and hydriding combustion synthesis (HCS) [45]. HCS has been developed especially for the preparation of Mg-based alloys with the merits of low energy consumption, short processing time, high activity of the product and simple experimental requirement. MM is an effective method for the preparation of nanocrystalline or amorphous Mg-based alloys with large grain boundaries as well as lattice defects.

In our previous studies, we combined the process of HCS and MM, i.e., HCS + MM to prepare binary Mg–Ni and ternary Mg–La–Ni composites [46,47], finding that the hydrogen storage properties

* Corresponding author at: College of Materials Science and Engineering, Nanjing University of Technology, 5 Xinmofan Road, Nanjing 210009, People's Republic of China. Tel.: +86 25 83587242.
E-mail address: yfzhu@njut.edu.cn (Y. Zhu).

0925-8388/$ – see front matter © 2012 Elsevier B.V. All rights reserved.
doi:10.1016/j.jallcom.2012.01.018

are improved remarkably as compared to the HCS product, suggesting that HCS + MM is promising to prepare advanced Mg-based hydrogen storage materials. However, it is not yet clear how about the effect of Fe on the hydrogen storage properties of Mg–Ni system prepared by the process of HCS + MM. Therefore, the aim of this study is to investigate the structural and hydrogen storage properties of ternary $Mg_{90}Ni_{10-x}Fe_x$ (x = 0, 2, 4, 6 and 8) composites prepared by HCS + MM.

2. Experimental

The metallic powders of Mg (99 wt.% in purity and <74 μm in diameter), Ni (99 wt.% in purity and 2–3 μm in diameter) and Fe (99.9 wt.% in purity and <74 μm in diameter) were commercially gotten. They were well-mixed in acetone with atomic compositions of $Mg_{90}Ni_{10-x}Fe_x$ (x = 0, 2, 4, 6 and 8) by an ultrasonic homogenizer for 60 min. After being completely dried at 323 K in air, the powder mixtures without any compressive treatment were used directly for HCS. During the HCS process, the samples were first heated up to 853 K at the rate of 7 K/min and held for 60 min under 1.9 MPa hydrogen pressure, then cooled down to 613 K and held for 120 min, and finally cooled down to room temperature. After HCS, the powders with 1 wt.% graphite as process control agent were mechanically milled together under 0.1 MPa argon atmospheres on a planetary ball mill with ball to powder ratio of 30:1 at 200 rpm for 600 min.

The crystal structures of the composites were examined by X-ray diffraction (XRD) with Cu-K_α radiation using ARL X'TRA diffractometer working at 45 kV and 35 mA. The surface morphologies of the composites were observed by scanning electron microscopy (SEM) equipped with an energy dispersive X-ray spectrometer (EDX).

The hydrogen storage properties of the composites were measured without any activation treatment using the Sievert's method by the gas reaction controller. The transfer of the samples to the sample chamber was operated in a glove box filled with argon atmosphere to prevent possible Mg oxidation. Before hydriding measurement, the composites were dehydrided completely under vacuum by heating up to approximately 603 K. Then the hydriding/dehydriding kinetics were measured in the temperature range from 373 K to 523 K. The initial hydrogen pressure was 3.0 MPa for hydriding and 0.005 MPa for dehydriding, respectively. To clarify the thermodynamic properties of the composites, the pressure-composition isotherms (PCIs) were measured at 523 K, 573 K and 623 K, respectively.

3. Results and discussion

3.1. Structural characterization

Fig. 1 shows the XRD patterns of the as-synthesized $Mg_{90}Ni_{10-x}Fe_x$ (x = 0, 2, 4, 6 and 8) composites before dehydrogenation. It can be seen that all of the composites include the phases of MgH_2, Mg_2NiH_4, $Mg_2NiH_{0.3}$ and Mg, and MgH_2 is the main phase supported by our previous study [46]. During the HCS process, hydrides of MgH_2, Mg_2NiH_4 and $Mg_2NiH_{0.3}$ were formed and part of Mg was not fully hydrogenated. With the addition of

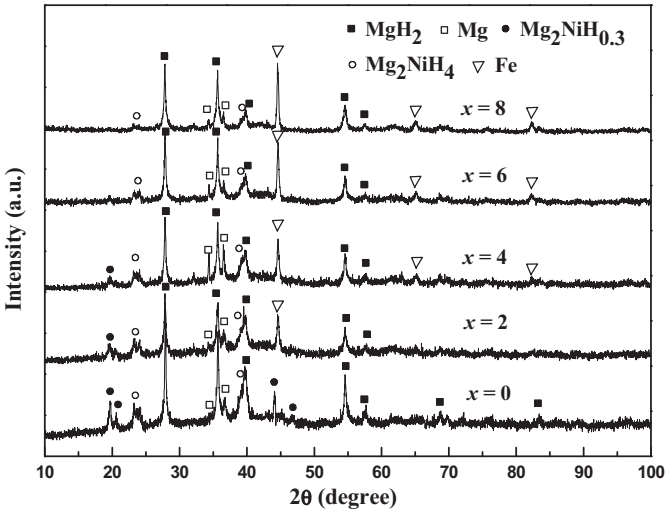

Fig. 1. XRD patterns of the $Mg_{90}Ni_{10-x}Fe_x$ (x =0, 2, 4, 6 and 8) composites.

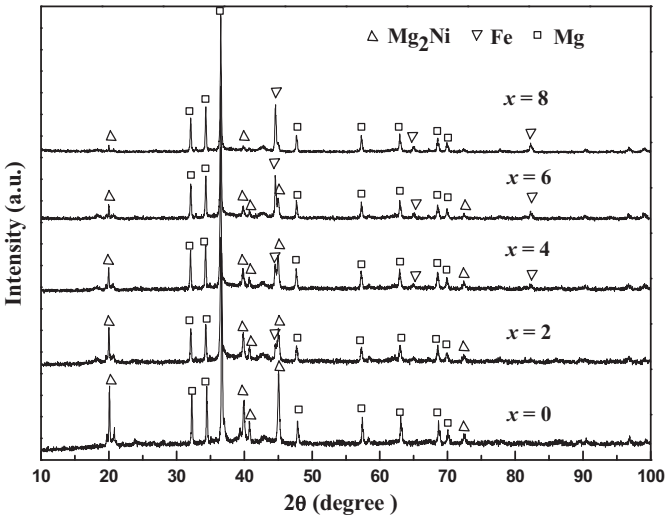

Fig. 2. XRD patterns of the $Mg_{90}Ni_{10-x}Fe_x$ (x = 0, 2, 4, 6 and 8) composites after dehydrogenation at 603 K.

Fe, the diffraction peaks of Fe appear in the patterns. Besides, the diffraction intensities of Fe increase with the increased amount of Fe, while the diffraction intensities of Mg_2NiH_4 are decreased, indicating that Fe did not participate in any chemical reaction with other substance during the period of HCS or MM. The average grain sizes of the main phase MgH_2 in the composites were estimated from the diffraction peaks of MgH_2 according to Scherrer's equation [48]:

$$D\beta\cos\theta = 0.9\lambda \quad (1)$$

where D is the grain size, λ is the X-ray wavelength of 0.154 nm, β is the full width at half maximum of the diffraction peak and θ is the Bragg angle. The average grain sizes of MgH_2 in the $Mg_{90}Ni_{10-x}Fe_x$ (x = 2, 4, 6 and 8) and $Mg_{90}Ni_{10}$ composites were estimated to be 25–30 nm and 40 nm, respectively. All of the composites have nanometer-scale structures due to the effect of MM on the brittle HCS products, and the addition of Fe is favorable to the reduction of grain size of MgH_2.

The XRD patterns of the five composites after dehydriding at 603 K are shown in Fig. 2, the dehydrogenated composites contain only Mg_2Ni, Mg and Fe, indicating that all the hydrogen in the hydrides can be fully desorbed at 603 K. Moreover, no reactions between Fe and Mg_2Ni or Mg are observed.

The SEM images of the $Mg_{90}Ni_{10-x}Fe_x$ (x = 0, 2, 4, 6 and 8) composites are shown in Fig. 3. Compared with the binary Mg–Ni system, the ternary Mg–Ni–Fe system possesses smaller and uniform particle size especially for the $Mg_{90}Ni_2Fe_8$ composite, indicating that the addition of Fe is also helpful for the particle refinement of the composites during the process of HCS and MM. Fig. 3(c, e, g, i) shows the EDS mapping of Fe on the same area of the corresponding secondary electron image. It can be seen that Fe distributes uniformly on the surface of the composites, and the distribution density is increased with increasing the Fe content in the composite.

3.2. Hydriding/dehydriding properties

As the $Mg_{90}Ni_{10-x}Fe_x$ (x = 0, 2, 4, 6 and 8) composites contained hydride phases, they were dehydrogenated completely at 603 K at first. Then the hydriding properties of these composites were investigated. The hydriding kinetic properties of these composites measured at 373 K and 493 K under 3.0 MPa hydrogen pressure are shown in Fig. 4. As can be seen in Fig. 4(a), $Mg_{90}Ni_2Fe_8$ exhibits the

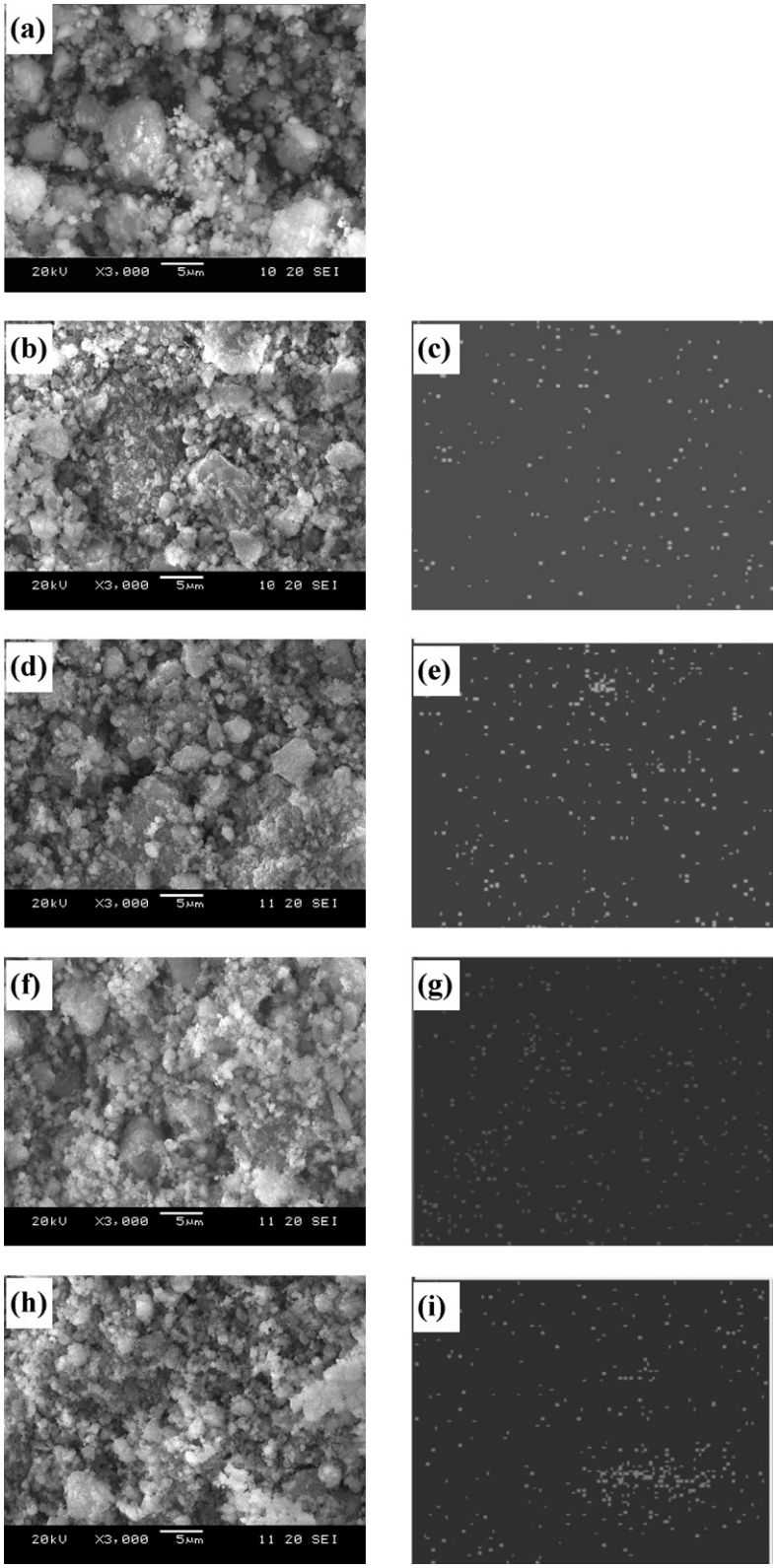

Fig. 3. SEM images of the composites with associated EDS maps for Fe: (a), (b), (d), (f) and (h) are secondary electron images with $x = 0, 2, 4, 6, 8$, respectively; (c), (e), (g) and (i) express the distribution of Fe with $x = 2, 4, 6, 8$, respectively.

best hydriding properties with the highest hydrogen capacity of 4.80 wt.% at 373 K, and only needs 30 s to absorb 97% of its saturated hydrogen capacity. However, $Mg_{90}Ni_{10}$ requires more than 100 s to reach its saturated hydrogen capacity of 4.30 wt.%. Based on the phase structures of the composites, the theoretical hydrogen storage capacity was calculated to be 6.49, 6.50, 6.51, 6.53 and 6.54 wt.% for the $Mg_{90}Ni_{10-x}Fe_x$ ($x = 0$, 2, 4, 6 and 8) composites, respectively. The theoretical hydrogen storage capacity of the composites changes little with Fe substitution for Ni. The difference between the experimental and theoretical hydriding capacity

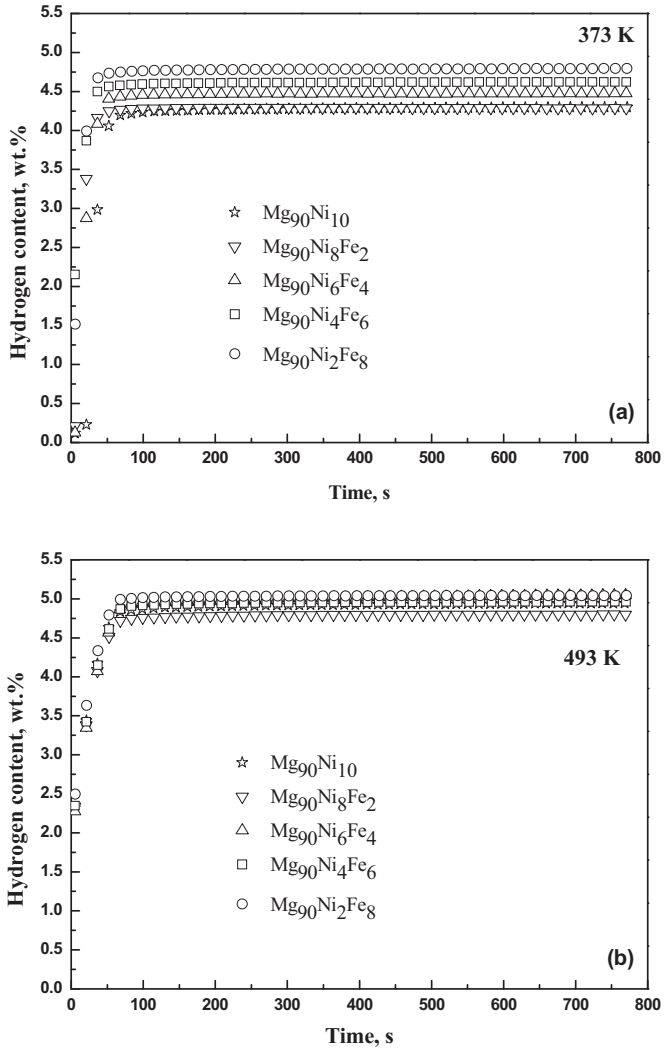

Fig. 4. Hydriding curves of the $Mg_{90}Ni_{10-x}Fe_x$ (x = 0, 2, 4, 6 and 8) composites measured at 373 K (a) and 493 K (b) under an initial hydrogen pressure of 3.0 MPa.

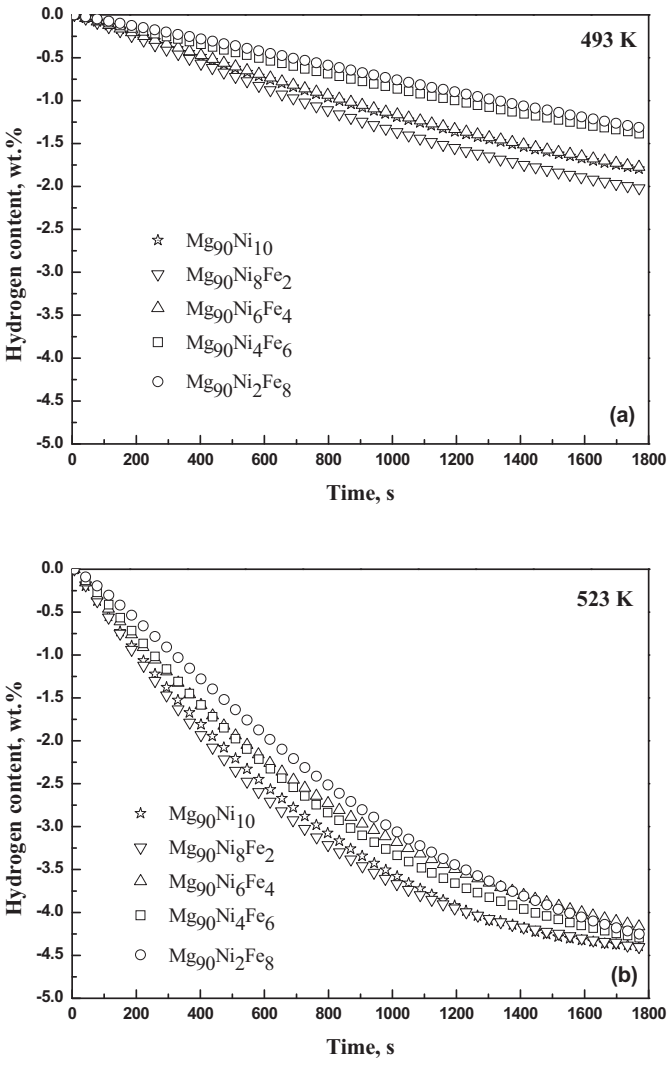

Fig. 5. Dehydriding curves of the $Mg_{90}Ni_{10-x}Fe_x$ (x = 0, 2, 4, 6 and 8) composites measured at 493 K (a) and 523 K (b) under an initial hydrogen pressure of 0.005 MPa.

of the composite is mainly due to the un-hydrogenated Mg during hydriding at 373 K. Besides, it is noticed that the hydriding rate and hydrogen absorption capacity of the composite increase with increasing the Fe content. The results indicate that the Mg–Ni–Fe composite has superior low temperature hydriding properties.

Increasing the hydriding temperature to 493 K, as shown in Fig. 4(b), the hydrogen absorption capacities of the composites are further increased, and the $Mg_{90}Ni_2Fe_8$ composite still shows the best hydriding properties with the highest hydrogen capacity of 5.04 wt.%.

Dehydriding kinetics of the $Mg_{90}Ni_{10-x}Fe_x$ (x = 0, 2, 4, 6 and 8) composites were investigated at 493 K and 523 K under an initial hydrogen pressure of 0.005 MPa and the results are shown in Fig. 5. The hydrogen desorption capacities within 1800 s of the composites are also listed in Table 1. At 493 K, all the composites can desorb hydrogen with a slow rate. Both of the dehydriding kinetics and hydrogen desorption capacities of the composites are improved when the temperature is increased to 523 K. Besides, it is found that the $Mg_{90}Ni_8Fe_2$ composite exhibits the best dehydriding properties among the five samples. For example, it desorbs the largest hydrogen capacity of 2.02 wt.% at 493 K and 4.40 wt.% at 523 K within 1800 s.

3.3. Thermodynamic properties

Fig. 6 presents the pressure-composition isotherms (PCIs) of the $Mg_{90}Ni_{10}$ and $Mg_{90}Ni_8Fe_2$ composites measured at 523, 573 and 623 K. Each isotherm exhibit two hydrogen absorption/desorption plateaus, in which the low pressure plateau corresponds to Mg, and the high pressure plateau corresponds to Mg_2Ni [49].

To obtain the thermodynamic parameters for hydrogenation/dehydrogenation of the composites, Fig. 7 gives the Van't Hoff plots for Mg and Mg_2Ni in the $Mg_{90}Ni_{10}$ and $Mg_{90}Ni_8Fe_2$ composites, and the calculated results are listed in Table 2. The enthalpies of dehydrogenation for MgH_2 and Mg_2NiH_4 in the $Mg_{90}Ni_{10}$ composite were calculated to be 79.1 kJ/mol and 66.2 kJ/mol, which are in agreement with the reported values [50]. After Fe substitution, the enthalpies and entropies of hydrogenation/dehydrogenation for Mg and Mg_2Ni in the $Mg_{90}Ni_8Fe_2$ composite changes little, as can be seen in Table 2. Thus, it can be concluded that the thermodynamic properties of the $Mg_{90}Ni_{10}$ composite are not altered by substitution of Fe for Ni. The improvement in hydriding/dehydriding properties of the Mg–Ni–Fe composite might be related to the micro-structural changes.

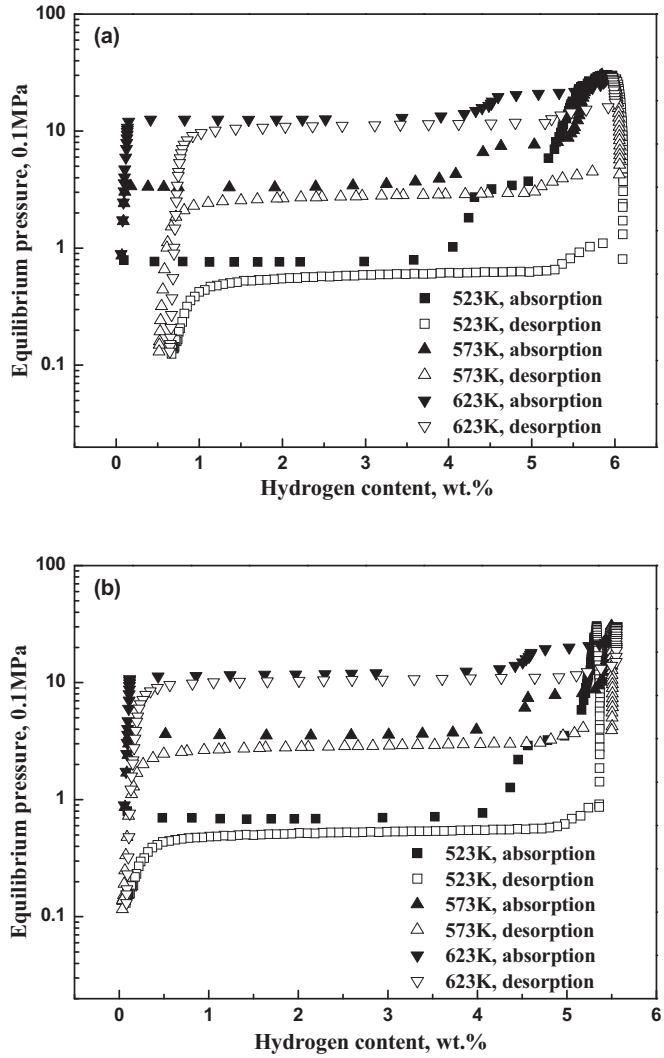

Fig. 6. Pressure-composition isotherms of $Mg_{90}Ni_{10}$ (a) and $Mg_{90}Ni_8Fe_2$ (b) measured at 523, 573 and 623 K.

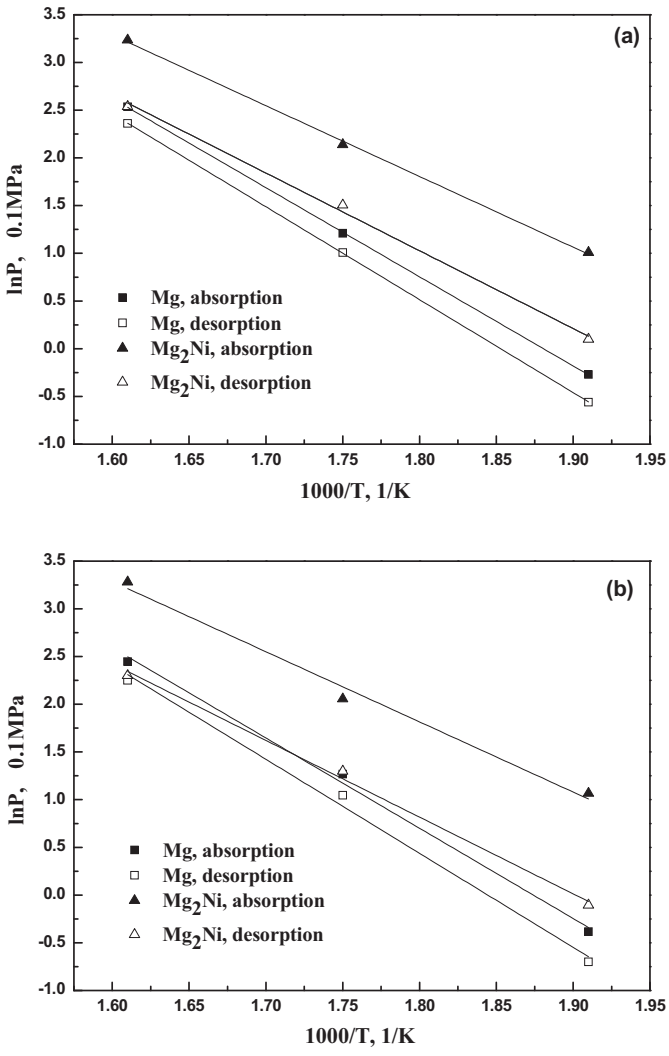

Fig. 7. Van't Hoff plots for Mg and Mg_2Ni in $Mg_{90}Ni_{10}$ (a) and $Mg_{90}Ni_8Fe_2$ (b).

3.4. Discussion

Based on the experimental results above, we can conclude that the technique of HCS + MM is appropriate for preparing Mg–Ni–Fe composites. The product has excellent hydrogen storage properties especially the hydriding kinetics partly related to the favorable microstructures. Firstly, the HCS product, which is the starting material for MM, is brittle and has many crystal defects and fresh surfaces evidenced by our previous study [51]. Secondly, after MM, the average grain size and particle size are both reduced and nanocrystalline structures are generated. The above factors are helpful for the dissociation/recombination of H_2 on the surface, increasing the active sites for reactions and shortening the hydrogen diffusion distance, leading to an improved hydriding/dehydriding properties.

Table 1
Hydrogen desorption capacities (wt.%) of the composites measured at 493 K and 523 K within 1800 s.

Temperature (K)	$Mg_{90}Ni_{10}$	$Mg_{90}Ni_8Fe_2$	$Mg_{90}Ni_6Fe_4$	$Mg_{90}Ni_4Fe_6$	$Mg_{90}Ni_2Fe_8$
493	1.79	2.02	1.77	1.38	1.31
523	4.39	4.40	4.16	4.29	4.25

Table 2
Thermodynamic parameters obtained from the Van't Hoff plots shown in Fig. 7 for $Mg_{90}Ni_{10}$ and $Mg_{90}Ni_8Fe_2$.

Sample	Phase	Hydriding		Dehydriding	
		$-\Delta H$ (kJ/mol)	$-\Delta S$ (J/mol K)	ΔH (kJ/mol)	ΔS (J/mol K)
$Mg_{90}Ni_{10}$	Mg	75.8	142.6	79.1	146.3
	Mg_2Ni	60.2	123.0	66.2	127.6
$Mg_{90}Ni_8Fe_2$	Mg	76.4	143.8	79.8	147.6
	Mg_2Ni	59.5	122.4	65.3	124.2

The phase of Mg_2Ni in the composite plays a catalytic role in enhancing the hydrogenation of Mg by promoting dissociation of hydrogen molecules on the surface [43]. Besides, as shown in Fig. 3(c, e, g, i), Fe distributes uniformly on the surface of the composites, which also has catalytic effect on improving the hydrogen storage properties. On the one hand, Fe addition results in grain and particle refinement of the composite as shown in Section 3.1, which increases the fraction of grain boundary and the specific surface area, favoring hydrogen adsorption/desorption on the surface and hydrogen diffusion in the bulk of the composite. On the other hand, the dispersed Fe may act as nuclear center of hydrogenation/dehydrogenation reactions during hydriding/dehydriding of the composite. With increasing the Fe content, the hydriding properties are improved and $Mg_{90}Ni_2Fe_8$ shows the best hydriding kinetics with the highest hydrogen capacity. This result indicates that Fe has better catalytic effect than Mg_2Ni on hydriding of the composite.

For dehydrogenation, the $Mg_{90}Ni_8Fe_2$ composite possesses the best dehydriding properties. Both of the dehydriding kinetics and capacity are decreased with increasing the Fe content ($x > 2$) although the hydriding capacity reaches the maximum for the $Mg_{90}Ni_2Fe_8$ composite. During dehydriding, Mg_2NiH_4 desorbs hydrogen first as it is thermodynamically less stable comparing with MgH_2 [52], promoting the dehydrogenation of adjacent MgH_2 phase. While proper amount of Fe addition ($x = 2$) is found also favorable to hydrogen desorption of the composite. In Section 3.3, we have concluded that the thermodynamic properties of the $Mg_{90}Ni_{10}$ composite are not altered with Fe addition. Therefore, we ascribe the superior dehydriding properties of the $Mg_{90}Ni_8Fe_2$ composite to the synergistic catalytic effects of Mg_2Ni and Fe phases.

4. Conclusion

Structures and hydrogen storage properties of the $Mg_{90}Ni_{10-x}Fe_x$ ($x = 0$, 2, 4, 6 and 8) composites prepared by HCS + MM were investigated. All of the composites show multiphase structures. Fe cannot react with Mg or Ni, and it distributes uniformly on the surface of the composites. XRD and SEM analyses show that Fe is favorable to grain and particle refinement of the composite. The composites have superior low temperature hydriding properties, and the $Mg_{90}Ni_2Fe_8$ composite exhibits the best hydriding properties, which absorbs 4.80 wt.% hydrogen at 373 K within 100 s. Fe has better catalytic effect than Mg_2Ni on hydriding of the composite. The best dehydriding properties are found for the $Mg_{90}Ni_8Fe_2$ composite, in which the Mg_2Ni and Fe phases have synergistic catalytic effects on hydrogen desorption. Furthermore, the addition of Fe cannot alter the thermodynamic properties of the $Mg_{90}Ni_{10}$ composite, but improves the hydriding/dehydriding kinetics of the composite.

Acknowledgments

This work was supported by National Natural Science Foundation of China (Nos. 51071085, 51171079), National 863 program (No. 2007AA05Z110), Natural Science Foundation of Jiangsu Province (No. BK2009361) and the Priority Academic Program Development of Jiangsu Higher Education Institutions (PAPD).

References

[1] L. Schlapbach, A. Züttel, Nature 414 (2001) 353.
[2] J.J.G. Willems, K.H.J. Buschow, J. Less-Common Met. 129 (1987) 13.
[3] H.G. Pan, R. Li, Y.F. Liu, M.X. Gao, H. Miao, Y.Q. Lei, Q.D. Wang, J. Alloys Compd. 463 (2008) 189.
[4] Y.F. Liu, Y.H. Cao, L. Huang, M.X. Gao, H.G. Pan, J. Alloys Compd. 509 (2011) 675.
[5] J. Matsuda, Y. Nakamura, E. Akiba, J. Alloys Compd. 509 (2011) 7498.
[6] K. Young, T. Ouchi, B. Huang, M.A. Fetcenko, J. Alloys Compd. 511 (2012) 242.
[7] M.X. Gao, S.C. Zhang, H. Miao, Y.F. Liu, H.G. Pan, J. Alloys Compd. 489 (2010) 552.
[8] Y.F. Liu, F.H. Wang, Y.H. Cao, M.X. Gao, H.G. Pan, Q.D. Wang, Energy Environ. Sci. 3 (2010) 645.
[9] R.V. Denys, V.A. Yartys, J. Alloys Compd. 509 (2011) S540.
[10] C. Liang, Y.F. Liu, H.L. Fu, Y.F. Ding, M.X. Gao, H.G. Pan, J. Alloys Compd. 509 (2011) 7844.
[11] Y.F. Liu, H.G. Pan, M.X. Gao, Q.D. Wang, J. Mater. Chem. 21 (2011) 4743.
[12] K.J. Jeon, H.R. Moon, A.M. Ruminski, B. Jiang, C. Kisielowski, R. Bardhan, J.J. Urban, Nat. Mater. 10 (2011) 286.
[13] L. Xie, Y. Liu, X.Z. Zhang, J.L. Qu, Y.T. Wang, X.G. Li, J. Alloys Compd. 482 (2009) 388.
[14] J. Bellemare, J. Huot, J. Alloys Compd. 512 (2012) 33.
[15] Y.F. Liu, K. Zhong, M.X. Gao, J.H. Wang, H.G. Pan, Q.D. Wang, Chem. Mater. 20 (2008) 3521.
[16] J.F. Stampfer, C.E. Holley, J.F. Suttle, J. Am. Chem. Soc. 82 (1960) 3504.
[17] Q. Luo, X.H. An, Y.B. Pan, X. Zhang, J.Y. Zhang, Q. Li, Int. J. Hydrogen Energy 35 (2010) 7842.
[18] E. Wirth, F. Munnik, L.L. Pranevičius, D. Milcius, J. Alloys Compd. 475 (2009) 917.
[19] S. Couillaud, E. Gaudin, J.L. Bobet, Intermetallics 19 (2011) 336.
[20] R.V. Denys, I.Y. Zavaliy, V. Paul-Boncour, V.V. Berezovets, I.V. Koval'chuk, A.B. Riabov, Intermetallics 18 (2010) 1579.
[21] Q.A. Zhang, H.Y. Wu, Mater. Chem. Phys. 94 (2005) 69.
[22] M.D. Riktor, S. Deledda, M. Herrich, O. Gutfleisch, H. Fjellvág, B.C. Hauback, Mater. Sci. Eng. B 158 (2009) 19.
[23] L.Z. Ouyang, H.W. Dong, C.H. Peng, L.X. Sun, M. Zhu, Int. J. Hydrogen Energy 32 (2007) 3929.
[24] Y. Zhang, Y. Tsushio, H. Enoki, E. Akiba, J. Alloys Compd. 393 (2005) 147.
[25] I.G. Fernández, G.O. Meyer, F.C. Gennari, J. Alloys Compd. 464 (2008) 111.
[26] J.F.R. Castro, S.F. Santos, A.L.M. Costa, A.R. Yavari, W.J. Botta, T.T. Ishikawa, J. Alloys Compd. 376 (2004) 251.
[27] C. Milanese, A. Girella, G. Bruni, P. Cofrancesco, V. Berbenni, P. Matteazzi, A. Marini, Intermetallics 18 (2010) 203.
[28] E. Grigorova, M. Khristov, M. Khrussanova, J.L. Bobet, P. Peshev, Int. J. Hydrogen Energy 30 (2005) 1099.
[29] J.L. Bobet, E. Grigorova, M. Khrussanova, M. Khristov, D. Radev, P. Peshev, J. Alloys Compd. 345 (2002) 280.
[30] I. Okonska, W. Iwasieczko, M. Jarzebski, M. Nowak, M. Jurczyk, Int. J. Hydrogen Energy 32 (2007) 4186.
[31] Y. Song, W.C. Zhang, R. Yang, Int. J. Hydrogen Energy 34 (2009) 1389.
[32] M.Y. Song, I.H. Kwon, S.N. Kwon, C.G. Park, H.R. Park, J.S. Bae, Int. J. Hydrogen Energy 31 (2006) 43.
[33] M. Porcu, A.K. Petford-Long, J.M. Sykes, J. Alloys Compd. 453 (2008) 341.
[34] M. Polanski, J. Bystrzycki, T. Plocinski, Int. J. Hydrogen Energy 33 (2008) 1859.
[35] D.L. Sun, H. Enoki, M. Bououdina, E. Akiba, J. Alloys Compd. 282 (1999) 252.
[36] H. Gu, Y.F. Zhu, L.Q. Li, J. Alloys Compd. 424 (2006) 382.
[37] R. Vijay, R. Sundaresan, M.P. Maiya, S.S. Murthy, Y. Fu, H.P. Klein, M. Groll, J. Alloys Compd. 384 (2004) 283.
[38] P. Wang, H.F. Zhang, B.Z. Ding, Z.Q. Hu, Acta Mater. 49 (2001) 921.
[39] V. Fuster, G. Urretavizcaya, F.J. Castro, J. Alloys Compd. 481 (2009) 673.
[40] A.D. Rud, A.M. Lakhnik, V.G. Ivanchenko, V.N. Uvarov, A.A. Shkola, V.A. Dekhtyarenko, L.I. Ivaschuk, N.I. Kuskova, Int. J. Hydrogen Energy 33 (2008) 1310.
[41] Y. Wu, W. Han, S.X. Zhou, M.V. Lototsky, J.K. Solberg, V.A. Yartys, J. Alloys Compd. 466 (2008) 176.
[42] C. Suryanarayana, Prog. Mater. Sci. 46 (2001) 1.
[43] A. Zaluska, L. Zaluski, J.O. Ström-Olsen, J. Alloys Compd. 289 (1999) 197.
[44] J. Huot, G. Liang, S. Boily, A.V. Neste, R. Schulz, J. Alloys Compd. 293–295 (1999) 495.
[45] T. Akiyama, H. Isogai, J. Yagi, J. Alloys Compd. 252 (1997) L1.
[46] X.F. Liu, Y.F. Zhu, L.Q. Li, Intermetallics 15 (2007) 1582.
[47] Y.F. Zhu, Y.F. Liu, H. Gu, L.Q. Li, J. Alloys Compd. 477 (2009) 440.
[48] Y. Kojima, Y. Kawai, T. Haga, J. Alloys Compd. 424 (2006) 294.
[49] G. Liang, J. Huot, S. Boily, A.V. Neste, R. Schulz, J. Alloys Compd. 297 (2000) 261.
[50] K. Tanaka, Y. Kanda, M. Furuhashi, K. Saito, K. Kuroda, H. Saka, J. Alloys Compd. 293–295 (1999) 521.
[51] D.M. Liu, Y.F. Zhu, L.Q. Li, Int. J. Hydrogen Energy 32 (2007) 2417.
[52] J.J. Reilly, R.H. Wiswall, Inorg. Chem. 7 (1968) 2254.